Evolution of the Fe-Co magnetism and magnetic proximity effects in alternate Fe/Co monolayers on nonmagnetic Cu₃Au(001)

L. Cabral ⬤,[1,*] W. A. A. Macedo ⬤,[2,†] and E. Z. da Silva ⬤[1,‡]

[1]*Institute of Physics "Gleb Wataghin," IFGW, State University of Campinas, 13083-859 Campinas, SP, Brazil*
[2]*Nuclear Technology Development Center, CDTN, 31270-901 Belo Horizonte, MG, Brazil*

Magnetic heterostructures with ferromagnetic/nonmagnetic interfaces are very interesting materials due to the possibility to switch the magnetization, to control the induced magnetic moment, and also due to interfacial effects. The tuning of the spin-orbit coupling in magnetic materials allows engineering new spintronic devices. Using density functional theory, the induced local magnetic moments in copper and gold surface atoms of Cu₃Au(001) due to the deposited alternate magnetic Fe and Co monolayers were studied. To observe the tuning mechanism, the spin density of the FeCo/Cu₃Au(001) as a function of the number of deposited magnetic monolayers was extensively investigated. The Fe/Co deposition induces a hybridization between electronic states of the magnetic and nonmagnetic interface atoms, generating a broadening in *d* bands of the deposited material, engineering the magnetic moments of the interface atoms. This observed hybridization elucidates the charge variation in the interface atoms for stacking sequences starting with Fe or with Co as the first magnetic layer in direct contact with the Cu₃Au(001) substrate. By performing the spin-charge density calculations, we demonstrated that this magnetic induction occurs only for the nonmagnetic Cu-Au atoms at the Cu₃Au(001) surface.

I. INTRODUCTION

Magnetic nanostructured materials are very relevant to technological applications [1,2], as sensing technologies [3], and memory devices [4], among others [5–7]. In ferromagnetic/nonmagnetic (FM/NM) heterostructures, the magnetic properties of the FM material are of fundamental importance, but also the induced magnetism of NM materials due to proximity with ferromagnets may play a significant role, and both aspects have been extensively studied [8]. It has been shown, for instance, that induced magnetic moments can affect the spin Hall effect, spin transport, and spin damping properties, and such effect can play an important role in the magnetization dynamics in layered heterostructures for new spintronics devices [9–11]. A better understanding of the evolution of the magnetism in FM/NM heterostructures certainly contributes to spintronics and related phenomena [12], and should lead to important improvements in these fields [13].

For ultrathin films and layered nanostructures, the possibility of tailoring the magnetic anisotropy has been a topic of particular scientific interest for a long time, since a large perpendicular magnetic anisotropy (PMA) is a key feature for spintronic devices [14–16]. For Fe-Co ultrathin films, the influence of alloy composition and tetragonal distortion on PMA, induced by epitaxial growth on NM substrates, has been intensively investigated [17–20]. The anisotropic magnetic

properties of FeCo alloys were also calculated by Kota and Sakura [21] using *ab initio* investigations, and their results show that besides the degree of tetragonal distortion, chemical ordering is also important for PMA [22–24]. The engineering of magnetic properties of FeCo-based structures can be achieved by controlling the thickness of the materials on the substrate [25,26], playing a key role in the dynamic magnetic properties [27]. Very recently, simulations for FeCo/Ir [28] have also shown that structural relaxations and chemical compositions are important in the coupling and magnetism of the Fe and Co atoms.

Cu and Cu-alloys in fcc-substrates are among the main NM surfaces often used for the epitaxial growth of 3*d* FM ultrathin films, to investigate magnetovolume and structural effects [29,30], exchange bias [31,32], and tuning of the magnetic anisotropy [33]. Ordered Cu₃Au(001) is one of the important NM substrates frequently used in the investigation of the correlation between the structural and magnetic properties of epitaxial FM 3*d* metal and alloy layered nanostructures [34,35]. It has been suggested as a promising substrate for the growth of ordered Fe/Co films with a large PMA [36], due to their interatomic distance [37].

The structural and magnetic properties of alternate Fe/Co monolayers epitaxially grown on Cu₃Au(001) [29,38], a system that results in chemically ordered Fe/Co ultrathin films with a tetragonally distorted L1₀ structure, have been previously studied [39–41]. In this system, the growth-induced ordering plays also an important role in the different contributions boosting PMA [42]. The pulsed laser deposition technique was used to epitaxially grow the magnetic L1₀ FeCo

---

*lcabral@ifi.unicamp.br
†wmacedo@cdtn.br
‡zacarias@ifi.unicamp.br

surface interspersed with Cu and Ni layers [43], where the magnetic moments (MMs) and the magnetic anisotropy are increased by replacing the Cu by Ni. The magnetic anisotropy in epitaxial Ni/Cu$_3$Au(001) thin films was modulated by inserting an ultrathin Cu interlayer, combined with strain fields [44].

For FeCo, their spin-orbit coupling (SOC) remains an intriguing challenging task and theoretical studies have been devoted to understand and to enhance the FeCo magnetic properties [18]. The SOC has a relativistic origin, coupling the spin and angular orbital MMs, giving rise to a spatial anisotropy. Taking into account SOC interaction, Kebaili *et al.* [28] investigated the spin and orbital MMs as a function of Fe-Co chemical composition.

The discovery of the spin Hall effect [45,46] opened up a wide field to design new spintronic devices [47,48]. Spin-orbit torques are an emerging technology to manipulate the spin and orbital magnetization, electronic transport, SOC, phonons, magnons, and polarons [49]. The spin MMs switching by applying external fields and bias in antiferromagnetic (AF) Mn$_2$Au are yielding promising theoretical and experimental studies [50–53]. The spin magnetization in magnetic MLs at room temperature by spin-orbit torques has been reported [54], allowing one to increase the spin-orbit torque efficiency in the light of surface anisotropy [55]. Spin injection at magnetic and NM interfaces is a ruling factor to modulate the electronic transport, where the geometrical stacking yields important studies and applications, as the spin mixing conductance [56]. Spin currents in layered magnetic nanostructures are generating scientific endeavors to engineer the spin-orbital Hall conductivity [57]. Moreover, AF materials are nowadays strong candidates for future spintronic and memory devices, and, in this field, Mn$_2$Au is one of the most promising antiferromagnet for real-world spintronics [58,59]. Therefore, new studies on magnetic induction in Au atoms by proximity effect at metallic interfaces may be relevant also for layered magnetic systems based in the AF Mn$_2$Au [52,53,60]. Magnetism of NM atoms at interfaces by proximity effects may influence the magnetic anisotropy and also the damping, and could eventually play an important role in the magnetization dynamics in magnetic heterostructures for technological applications [61].

The hybridization of *d* orbitals by the proximity effects at a FM/NM interface influences the electronic and magnetic properties of both materials, and the NM can become FM in thin films and multilayers where the density of states is enhanced by band narrowing [62,63]. Hybridization with Co gives rise to a magnetic moment in the interfacial atoms of the noble metals Cu, Ag, and Au [64–66]. An induced magnetization has been observed in Cu atoms in layered systems like Fe/Cu [67], FeCo/Cu [42], Co/Cu [68], Gd/Cu [69], or CoPt/Cu [70] multilayers, and also in Cu nanoparticles embedded in Co [71]. There are different studies on induced spin polarization in metallic Au atoms in Fe/Au multilayers [72,73], and also a recent report on spin polarization of Cu (and Au) atoms in five-ML (monolayer) Fe-Co/Cu$_3$Au(001) [74].

The theoretical investigations at atomistic level based on *ab initio* density functional theory (DFT) are an efficient tool to understand and predict new properties of the interaction be-

tween the FeCo FM and NM systems. Also, DFT calculations were used to understand the experimental results of induced MMs in the Cu layer inserted between Co and Pt materials, where the coupling between the d_{xz} and d_{yz} above and below Fermi energy raises the perpendicular anisotropy [30]; however, the authors noted that the induced orbital MMs and the copper density of states near the Fermi level are quite small, suggesting that the Stoner [75] conditions for ferromagnetism are not satisfied for Cu and the proximity effects are a key factor to induce the MM in the copper layer.

Although recent works studying the magnetism of alternate Fe/Co monolayers (5 ML) grown on NM Cu$_3$Au(001) were reported [41,74], a ML-resolved study of the Fe and Co magnetism, and a deep understanding of the hybridization between the electronic states of the magnetic Fe/Co layers and the NM surface of the Cu$_3$Au(001) system is not yet presented. Besides the evolution of the Fe/Co magnetism, our aim is to also present the study of the influence of Fe and Co MLs on the Cu$_3$Au(001) substrate, since NM Cu$_3$Au(001) is a material that has been experimentally used as an interesting substrate often used for epitaxial growth of magnetic layers [41,44,74]. Investigations motivated by experimental results allowed us to obtain a deep understanding of the induced local magnetization.

The structure of the present work is as follows: theoretical and computational details are presented in Sec. II. The constructed epitaxial structures are displayed in Sec. III. The effect of the magnetic MLs deposition is presented in a comparative way with the pristine NM surface and with the cases of the freestanding Fe and Co monolayers and the FeCo freestanding double layer. A detailed discussion of the electronic structure, which describes the evolution of the magnetic moments in the alternate Fe and Co MLs deposition on the Cu$_3$Au(001) substrate, and the magnetic induction in the NM Cu and Au interface atoms is presented. Spin-resolved density of states and Bader charges are also discussed to further clarify the structures studied. Finally, in Sec. IV are presented the conclusions of this study.

II. THEORETICAL APPROACH AND COMPUTATIONAL DETAILS

The present work employs *ab initio* simulations based on density functional theory [76] within the spin-polarized generalized gradient approximation (GGA) [77] with the Perdew-Burke-Erzenhof (PBE) exchange-correlation energy functional [78,79], which provides an accurate description of the studied properties of the system in focus, such as lattice parameters and evolution of MMs [80,81]. The Kohn-Sham equations were solved using the projector augmented-wave (PAW) method [82,83], as implemented in the Vienna *ab initio* simulation package (VASP), version 5.4.4 [84,85], which is used to describe the electron-ion interactions with the PAW projectors Au($5d^{10}6s^1$), Cu($3d^{10}4s^1$), Fe($3d^74s^1$), and Co($3d^44s^1$), where the valence states are shown in parentheses. The calculated geometries of auricupride (Cu$_3$Au), iron (Fe), and cobalt (Co) were obtained by using the scalar-relativistic approximation to describe the valence electrons, i.e., the spin-orbit coupling was not taken into account for the valence states. However, the SOC within the noncollinear spin

methodology was introduced in our studies [86] to investigate the magnetic properties [87], as suggested by Andersen [88].

The *ab initio* modeling carried out in this work addressed questions raised by chemical order, i.e., alternate deposition of epitaxial Fe and Co MLs on $Cu_3Au(001)$. Within this framework, the challenging task is to understand and compute the interface properties between the NM layer and deposited magnetic MLs. From experimental observations, the iron and cobalt are grown layer by layer on Cu_3Au [41]. In bulk form, Cu_3Au shows a fcc structure, while both, iron and cobalt, present bcc geometries. Our calculations use the $Cu_3Au(001)$ surface to deposit a sequence of alternate magnetic MLs because this $Cu_3Au(001)$ surface offers an interesting template in which epitaxial MLs can be deposited, following the same stacking of the $Cu_3Au(001)$, namely, the first deposited layer stacks as the Cu layer, the second as the top $Cu_3Au(001)$, keeping registry with the $Cu_3Au(001)$ lattice spacing.

In order to understand the interface properties of $Fe(Co)/Cu_3Au(001)$, the equilibrium bulk structures were first calculated, and hence, atomic force relaxations. For the surfaces, only atomic forces are calculated. The equilibrium geometries for the Cu_3Au, Fe, and Co bulk structures were obtained by the minimization of the stress tensor by using a plane waves extension cutoff of 800 eV, while for atomic forces optimization 466 eV was employed, which is 12.5% larger than the cutoff energies recommended by the VASP package. The number of plane waves used in the stress tensor minimizations (atomic force optimizations) increases (decreases) the computational cost of the computation. For the Brillouin zone integration, we used a **k** mesh of $9 \times 9 \times 9$ for the cubic bulk and $9 \times 9 \times 1$ for the surfaces in the optimizations, while double of these values were used for the electronic properties, such as density of states and charge density investigations. The Gaussian smearing method of 0.01 eV was employed to define the electronic states occupation, and 10^{-7} eV was adopted as the self-consistent electronic convergence criterion, where the equilibrium geometries were reached when all the forces were smaller than the $0.008 \, eV\,Å^{-1}$ on every atom. To characterize the spin interactions due to the stacking of the magnetic MLs on the NM layer, the difference between the minority and majority spins ($\Delta\rho\uparrow\downarrow = \rho\uparrow - \rho\downarrow$) were calculated.

A systematic study was undertaken, in order to understand the effect of the alternate deposition of magnetic MLs of Fe and Co on the (001) surface of Cu_3Au. The interesting epitaxial new systems constructed in this exercise allows the comparison with some experimental results performed in such systems [41,74]. First, the equilibrium lattice constants for Cu_3Au, Fe, and Co in bulk phases were converged to 3.78, 2.83, and 2.80 Å, respectively. The $Cu_3Au(001)$ surface provides a very interesting template to grow layered materials, in particular magnetic materials, such as Fe and Co. The structure of such surface offers geometrical constraints to the deposited layers, providing interesting geometrical and magnetic behavior. The $Cu_3Au(001)$ structure is a stacking sequence of alternate Au-Cu and Cu-Cu layers. The deposition of magnetic MLs on this surface also offers some interesting geometrical guides to the newly formed structures. The first deposited ML (and all odd MLs) stacks similarly to the Cu-Cu layer, while the second and the even layers stack as Cu-Au

planes. The $Cu_3Au(001)$ surface was modeled by a fcc[001] slab converged using spin-polarized calculations with 5 Au and 13 Ce, resulting in 18 atoms, where the slab terminations are composed by Au-Cu in a nine-layer symmetric structure. The iron and cobalt were also calculated in the (001) surface, where each magnetic ML was simulated with only two atoms of the same species, Fe and Co. This geometrical ordering influences how the MMs behave. This work considers the experimental situation where the $Cu_3Au(001)$ surface is used as a template to force the deposited MLs to have the same stacking of the underlying structure and forcing them to the $Cu_3Au(001)$ lattice spacing separation with consequences to their magnetic behavior.

III. RESULTS

To understand the effect of the deposition of magnetic MLs on the Cu_3Au surface, freestanding MLs of Fe and Co with interatomic spacing ($d_{a-a} = 2.67$ Å), provided by the Cu_3Au surface template, were calculated. These MLs with MMs (Fe ML = 3.09 μ_B and Co ML = 2.10 μ_B) should be upper limits for the MMs of the deposited MLs, since they are freestanding. Freestanding FeCo double layer with MMs (Fe DL = 2.75 μ_B and Co DL = 1.66 μ_B) were also calculated, which should also be upper bounds for the FeCo and CoFe deposited double layers (DLs), following the same reasons. After this exercise, the magnetic behavior of the alternate Fe and Co MLs deposited on the $Cu_3Au(001)$, up to a total thickness of six MLs, was investigated. Figure 1 shows some of the studied structures, where gold, copper, iron, and cobalt atoms are shown in yellow, brown, red, and blue, respectively. The positive isosurface used in these images was $13.8 \, e\,Å^{-3}$, represented by blue.

A. Layer-by-layer deposition of Fe/Co and induced magnetization in Cu and Au atoms

In Fig. 2, the relaxed $Cu_3Au(001)$ surface is presented. In the clean substrate, the surface copper atom suffers a displacement of 0.17 Å in the out-of-plane direction in comparison with the gold in-plane positions, shown in the left panel. With the deposition of one ML of Fe(001), the equilibrium position of the Cu surface atoms returns to the in-plane position of the Au atoms, as shown in the right panel. These findings are in good agreement with Ref. [89].

Therefore, the deposited magnetic material aligns the Au-Cu atoms of the interface and also adjusts the interplanar distance between the top and bottom layers. In addition, the first deposited Fe (Co) magnetic ML, which has a Cu-type stacking on $Cu_3Au(001)$, converged to a vertical distance of 1.90 Å (1.85 Å) from the NM surface. For the two layers FeCo (CoFe), the distance between the magnetic layer and the NM ML was 1.96 Å (1.93 Å), where the MLs are separated by 1.44 Å (1.39 Å). For FeCoFe (CoFeCo), three magnetic MLs, the distance between the first magnetic ML and the NM surface, is 1.95 Å (1.80 Å), where the distances between the magnetic atoms are $d^{Fe-Co} = 1.66$ Å and $d^{Co-Fe} = 1.45$ Å ($d^{Co-Fe} = 1.54$ Å and $d^{Fe-Co} = 1.46$ Å). The different converged vertical distances from iron and cobalt to the $Cu_3Au(001)$ surface influence the hybridization between
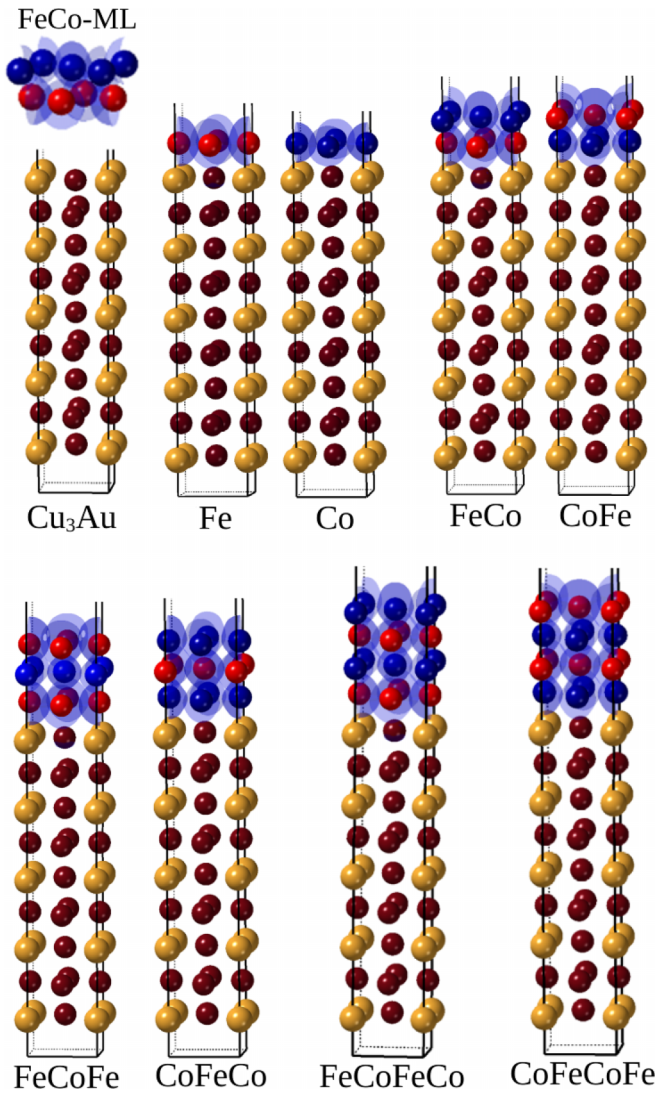
FIG. 1. Calculated structures and magnetic isosurface for the FeCo free-double layer, Cu$_3$Au(001), and the sequence of alternate magnetic MLs (Fe, Co) deposited on the NM substrate: Fe(001), Co(001), FeCo(001), CoFe(001), FeCoFe(001), CoFeCo(001), FeCoFeCo(001), and CoFeCoFe(001). The used isosurface is 13.8 $e\,$Å^{-3}, shown in blue.

FIG. 2. In the left panel is represented the free Cu$_3$Au(001) surface, and in the right panel is shown the Cu$_3$Au(001) surface with one-ML Fe deposited. The DFT calculation indicates, for the free Cu$_3$Au(001), a corrugation of 0.17 Å.

the Cu/Au surface atoms and Fe/Co overlayer charge densities, which induces magnetism in the NM interface atoms. The induced MM is higher in the copper than in the gold surface atoms due to their occupied d states near the Fermi energy. Also, this behavior of the d-copper and d-gold surface atoms with and without the iron-cobalt MLs is due to the hybridization with d states of the magnetic material, which can be varied with the increase in the number of magnetic MLs.

To further understand the trends and evolution of the magnetic properties of the deposited magnetic layers and their effect on the Cu$_3$Au interface atoms, the LDOS, per atom, were calculated for freestanding MLs and for depositions of single layers of Fe(001) and Co(001), as presented in Fig. 4, and also the freestanding DL and for DL depositions (Fe/Co and Co/Fe) on the Cu$_3$Au(001), shown in Fig. 5. In these figures, the yellow panels denote the LDOS for free-ML and DL atoms; gray color panels, the deposited magnetic MLs; and, in cyan, the bottom panels depict the copper and gold surface atoms. The red (blue) line identifies the iron (cobalt). The freestanding MLs show higher LDOS intensity (Fig. 4)

the NM and magnetic interface atoms, allowing one to study the tuning of the MMs of the interface atoms.

To understand the effect of the deposition of magnetic MLs on the NM Cu$_3$Au(001) surface, the local density of states (LDOS) for the surfaces with and without the deposited magnetic double-layer FeCo(001) were calculated, as depicted in Fig. 3, where the upper panels show the average LDOS, per atom, for all copper (d-Cu states, left panel) and gold (d-Au states, right panel), whereas the bottom panels show the LDOS for the surface copper (d-Cu-T, in the left) and gold ML (d-Au-T, in the right). These figures show the influence of the magnetic materials on the copper and gold states. There is a clear shift of both Cu and Au LDOS to lower energies with respect to the Fermi energy (blue), as compared with the Cu$_3$Au(001) in the absence of the magnetic material (red). This significant difference is due to the interaction between
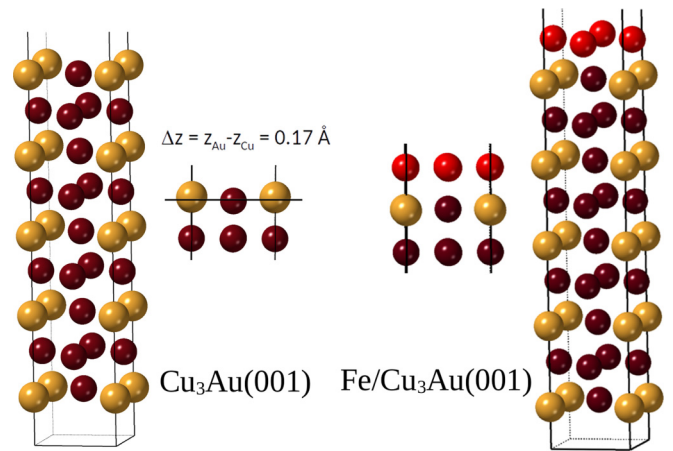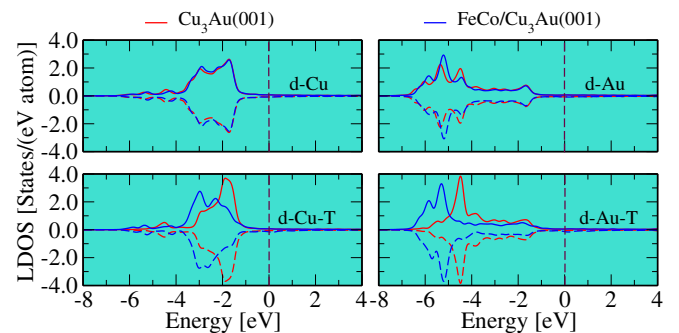

FIG. 3. Local density of states, per atom. In the upper panels, the d-Cu and d-Au state contributions from all slab atoms. In the bottom panels, the copper (d-Cu-T) and gold (d-Au-T) surface atoms of Cu$_3$Au(100). The calculations were performed in the absence (red) and presence (blue) of the FeCo(100) magnetic MLs.
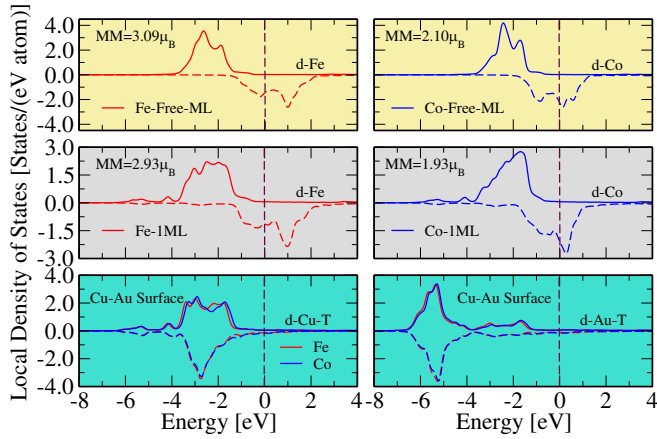
FIG. 4. Local density of states per atom and the spin MMs for (upper panels) freestanding Fe(001) and Co(001) MLs; (center panels) d-Fe and d-Co deposited ML atoms; and (bottom panels) the LDOS for Cu$_3$Au(100) surface atoms, d-Cu-T and d-Au-T. Red lines for Fe(001) and blue lines for Co(001) depositions.

in comparison with the single deposited magnetic MLs. Also, the calculated MM of 3.09 μ_B (2.10 μ_B) for the free Fe (Co) contrasts with the 2.93 μ_B (1.93 μ_B) MM of the deposited magnetic atoms, which evidence the effect of the hybridization between the deposited Fe/Co and the Cu$_3$Au(001) surface atoms.

In the case of the deposited DLs (Fig. 5), the Fe/Co and Co/Fe free-DL LDOS depicted in the top panel contrast with the deposited MLs. In the case of deposited FeCo (left panel) magnetic MLs, the hybridization of Fe with the NM surface and second deposited Co ML provides a decrease of its MM (2.60 μ_B), while the top Co ML with a free surface, hybridizes differently with the sandwiched first Fe layer, showing a
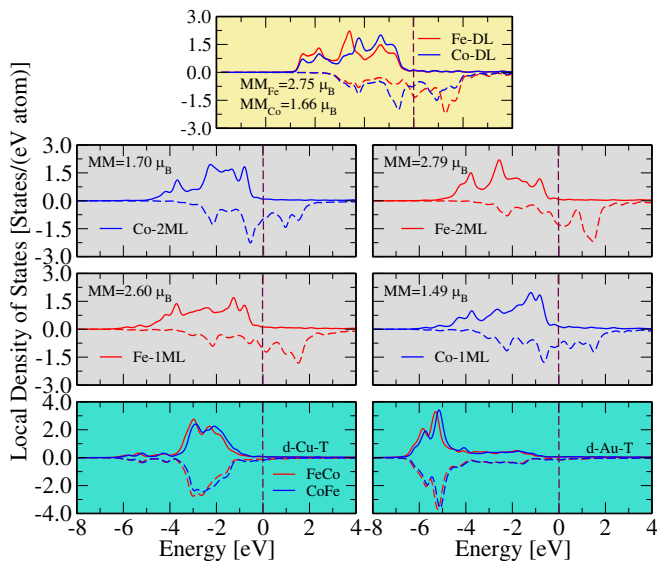

FIG. 5. Local density of states and spin MM for (upper panel) freestanding DL; (gray panels) FeCo(001) and CoFe(001) MLs deposited on Cu$_3$Au(100); and (bottom panels) d-Cu-T and d-Au-T, following the stacking order of the calculated surface. Red lines for FeCo and blue lines for CoFe depositions.
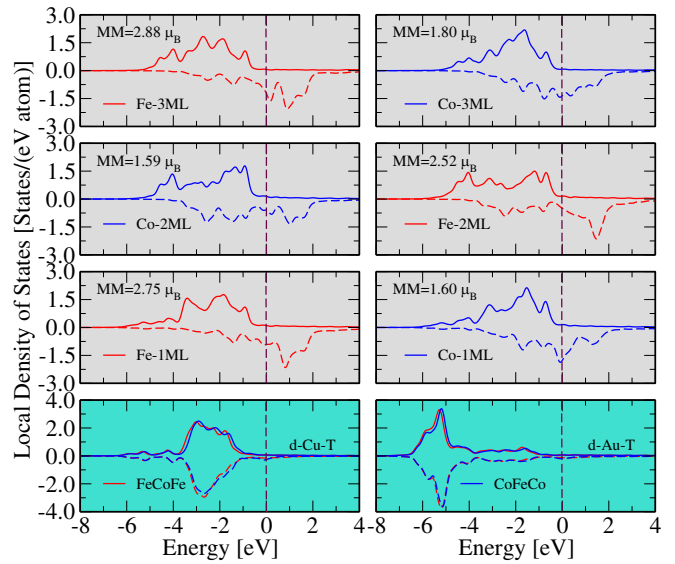

FIG. 6. LDOS for FeCoFe(100) (left gray panels) and CoFeCo(100) (right gray panels) stacked as the deposited. The bottom panels depict the LDOS for the copper and gold atoms of the Cu$_3$Au(100) interface. Red lines for FeCoFe and blue lines for CoFeCo depositions.

higher MM (1.70 μ_B). The case of deposited CoFe (right panel) is similar, the Co ML lowers its MM to 1.49 μ_B, while the iron MM in the second layer is increased.

The two cases discussed so far have a very interesting comparison indicated by the behavior of the freestanding ML and DL. The d-band widths of the freestanding ML and DL are determinant to the behavior of their deposited counterparts. Since Cu, and especially Au, have larger d-band widths, the hybridization with the single ML is less effective than the case of the DL. The hybridization of CoFe in the free-DL presents larger d-band width, which signals that this is a dominant factor influencing the effects of the DL deposition on the Cu$_3$Au(100). Therefore, the information from the freestanding cases, although hypothetical structures, helps the understanding that the hybridization of the magnetic MLs with the surface upon deposition is strongly influenced by their pure magnetic effect and the hybridization inducing MMs in the Cu and Au interface atoms is enhanced in the case of the free DL.

In the cases of three and four alternate Fe/Co MLs, depicted in Figs. 6 and 7, along with the previous ones show an overall tendency. The odd numbered structures have the MM for the first ML smaller than the free ML, but enhanced when compared with the even structures, and their top layer with a free surface also displays larger MMs. In the case of an odd number of deposited layers, the MM starts higher and the top layer is always higher than the even cases. This is a result of different hybridization between the d-Fe and d-Co with the Cu$_3$Au(001) atoms, shown in the upper panels of Figs. 6 and 7. The interaction with the surface atoms changes the electronic distribution of the magnetic atoms, providing a widening in the local density of states in the energy region of the d-Fe and d-Co electronic states. The interaction with the surface lowers the average MM as compared with either of the free
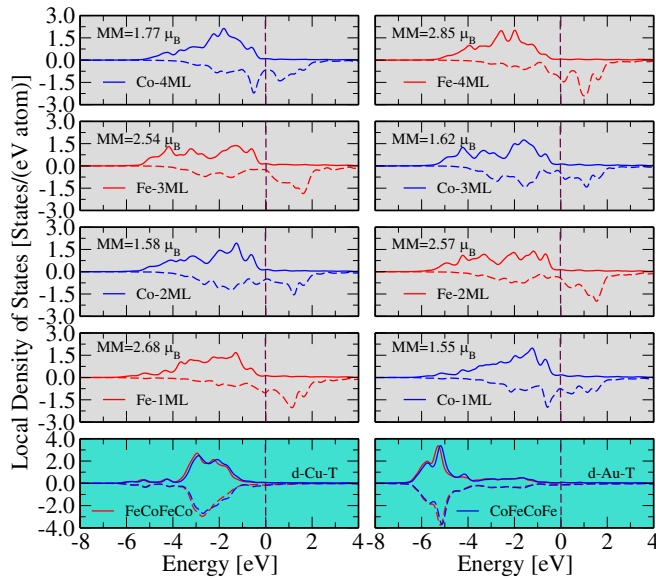
FIG. 7. The gray upper panels present, in the left (right), the local density of states per atom of each deposited ML, starting with Fe (Co). The bottom panels show the local density of states for the copper (left) and gold (right) surface MLs calculated with the FeCoFeCo (red) and CoFeCoFe(001) (blue) deposited magnetic MLs.

FIG. 8. Evolution of the spin MM for Cu and Au atoms of the $Cu_3Au(001)$ substrate, and for the Fe/Co MLs. In the left (right) panels, the magnetic ML in direct contact with the NM substrate is composed by Fe (Co) atoms.

MLs. Also, both calculations introduce differences between the minority and majority spins, that induced localized MM for the copper and gold interface atoms. By increasing the number of magnetic MLs, the induced MM varies according to the interface atoms. Thus, the increase in the number of magnetic MLs induces a stronger localized MM in the cooper and gold interface atoms, as well as provokes the tuning of the magnetic properties of the iron and cobalt, depending on the first ML. The details for four Fe/Co MLs are shown in Fig. 7.

The case of three MLs deposition of FeCoFe (CoFeCo), shows an increase in the MM values of the first and third layers, and the second ML has lower its MM due to interaction at both sides. In the case of FeCoFe, the spin MMs for in-plane iron are $2.75\,\mu_B$ and $2.88\,\mu_B$ and for Co is $1.59\,\mu_B$. For CoFeCo, the spin MMs for in-plane Co are $1.60\,\mu_B$ and $1.80\,\mu_B$ and for the middle Fe ML $2.52\,\mu_B$. The average MM values for each atom type, obtained with these stackings are $2.82\,\mu_B$ for Fe and $1.59\,\mu_B$ for Co for the case of FeCoFe, and $2.52\,\mu_B$ for Fe and $1.70\,\mu_B$ for Co in the case of CoFeCo.

For the four deposited MLs, namely, FeCoFeCo and CoFe-CoFe, the structure with Fe as first layer, the spin MMs for in-plane Fe are $2.68\,\mu_B$ and $2.54\,\mu_B$, while the spin MMs for in-plane Co are $1.58\,\mu_B$ and $1.77\,\mu_B$. In the structure with Co as first layer, the spin MMs for in-plane Fe are $2.57\,\mu_B$ and $2.85\,\mu_B$, while the spin MMs for in-plane Co are $1.55\,\mu_B$ and $1.62\,\mu_B$. Note that, in both structures, the first and top MLs tend always to higher values than the intermediate MLs, that tend to maintain similar values of MMs. These MMs give average values $2.61\,\mu_B$ for Fe and $1.68\,\mu_B$ for Co in the case of FeCoFeCo and Fe $2.71\,\mu_B$ and Co $1.58\,\mu_B$ in the case of CoFeCoFe.

It is interesting to note that, in the case of an odd number of deposited layers, the MM starts higher and the top layer is always higher than the even cases. The Cu shows
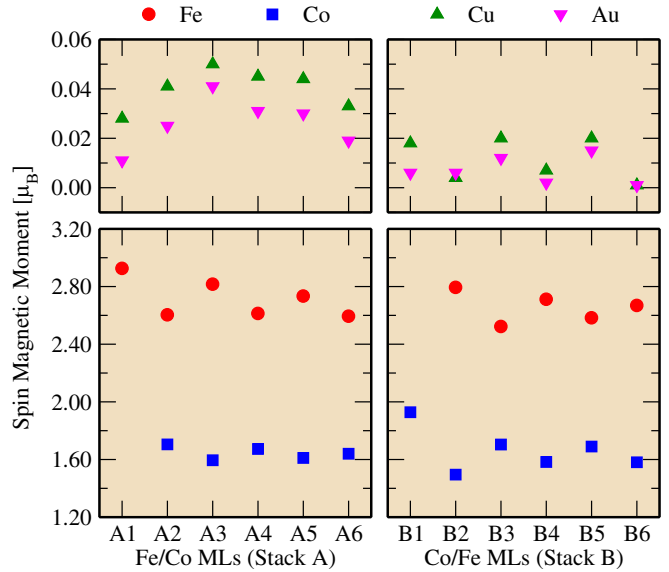
higher interaction with the magnetic MLs than the Au atoms, independent of chemical order, and it is stronger when the first ML is composed by Fe atoms.

The overall behavior of the MM evolution for increasing Fe/Co stacking displays some interesting features. It has some geometrical trends. Odd structures show the highest MM in the first and topmost layers as compared to the even numbered structures. The first ML interacts with the $Cu_3Au(100)$. The intermediary magnetic MLs interact with the other magnetic species, tending to show MM values in the range of $2.50 \pm 0.02\,\mu_B$ for the Fe MLs, and $1.6 \pm 0.02\,\mu_B$ for Co MLs. The topmost magnetic ML has always the higher MM since it has a free surface, but odd number MLs have higher MMs for the topmost ML. Due to the small interlayer distances, the magnetic MLs induce a local MM in the copper and gold interface atoms, where these induced MMs vary with the number and the chemical order of magnetic MLs. In this sense, we can induce and tune a localized MM in the copper and gold interface atoms and in the magnetic atoms. The first deposited magnetic ML has a stronger hybridization with the copper and gold surface ML. The second magnetic ML interacts mainly with the first and third magnetic MLs, which is similar for more layers. Thus, the stacking sequence order allows one to tune the induced MM.

The full evolution of the average MM, per atom type, upon stacking sequences of the deposited magnetic MLs, starting either with Fe or Co as the first magnetic ML in direct contact with the $Cu_3Au(001)$ substrate, can be seen in Fig. 8. These are very relevant results since they are the values that can be compared with experimental results from x-ray absorption spectroscopy and x-ray magnetic circular dichroism (XMCD) measurements. The bottom-left panel indicates the structures starting with the Fe ML (Stack A), from one (A1) up to six (A6) Fe/Co MLs. In these cases, the behavior of the Fe MM oscillates showing higher values when this is the

top layer but displaying an overall decreasing behavior with the increasing number of alternate Fe MLs. The behavior for Co MLs is similar. The bottom-right panel presents the structures starting with the Co ML (Stack B), from one (B1) up to six (B6) MLs. The overall behavior of the Fe and Co magnetization follows the same trends, but the Co average MM shows a higher oscillation. The top panels of Fig. 8 show the induced MMs for the Cu and Au interface atoms. In the top-left panel, the induced MM for the copper and gold surface atoms increases up to three magnetic MLs, which is the FeCoFe structure, the structure where the first and the last magnetic MLs are composed by Fe atoms, and then starts to decrease. The right panel, associated with structures starting with Co, shows an oscillating behavior. This behavior follows the oscillation of the total MM due to the Co atoms, which is higher for one (Co), three (CoFeCo), and five (CoFeCoFeCo) deposited MLs. The spin-charge density is more localized for Co than for Fe, therefore the effect of the first magnetic ML is dominant in these cases. In addition, in the top-right panel, the stronger MM is reached when the stacking is composed by three magnetic MLs, CoFeCo. Therefore, in both cases, the three MLs induce the highest MMs in Cu and Au, and in these cases, the Cu MM is always larger than the Au MM.

For the magnetic moments, the results of our calculations are in good agreement with the experiments for five alternate FeCo MLs epitaxially grown on Cu$_3$Au(001) [74], where it was reported that the experimental $3d$-spin MMs average, at 300 K, for Fe, Co, and Cu, when the first ML is composed by iron, are 2.11 μ_B, 1.50 μ_B, and 0.02 μ_B, respectively. The calculated $3d$-spin MMs (0 K) are 2.75 μ_B, 1.69 μ_B, and 0.07 μ_B. When the first ML is composed by cobalt, the obtained $3d$-spin MMs at 300 K are 2.05 μ_B, 1.47 μ_B, and 0.02 μ_B, while measurements at 30 K gave 2.43 μ_B, 1.70 μ_B, and 0.02 μ_B, and the theoretical values at 0 K are 2.63 μ_B, 1.73 μ_B, and 0.04 μ_B. The XMCD and DFT for the in-plane orbital MMs also show a good agreement, where 0.15 μ_B (0.19 μ_B), 0.25 μ_B (0.27 μ_B), and 0.001 μ_B (−0.001 μ_B) are the experimental measurements at 300 K when the Fe (Co) are in the first deposited ML, while 0.25 μ_B, 0.34 μ_B, and −0.002 μ_B measured at 30 K when the cobalt is at the interface. Also, 0.07 μ_B (0.06 μ_B), 0.07 μ_B (0.09 μ_B), and 0.001 μ_B (−0.002 μ_B) are the theoretical results for Fe, Co, and Cu with iron (cobalt) at the interface. DFT calculations obtained s- and p-Fe/Co spin states with antiferromagnetic alignment with respect to the d states in the case of the magnetic atoms, which contributed to the total MM. From the experimental results, in the particular case of Co, performed for two temperatures, it is clear that the calculated values (0 K) have to be larger. Considering this point, the comparison between the experiments and theory was rather satisfactory.

For six-ML Fe/Co on Cu$_3$Au(001), the authors in Ref. [41] measured the spin (orbital) MMs at room temperature and obtained 2.13 μ_B (0.29 μ_B) and 1.57 μ_B (0.33 μ_B), while our theoretical findings are 2.59 μ_B (0.06 μ_B) and 1.58 μ_B (0.07 μ_B), respectively. More details can be found in the Supplemental Material [90], where Table S1 reports the average of MM per ML and Table S2 reports the spin and orbital MM average, up to six ML Fe/Co.

Figure 9 represents the calculated work function for the clean Cu$_3$Au(001) surface (red line) and with deposition of
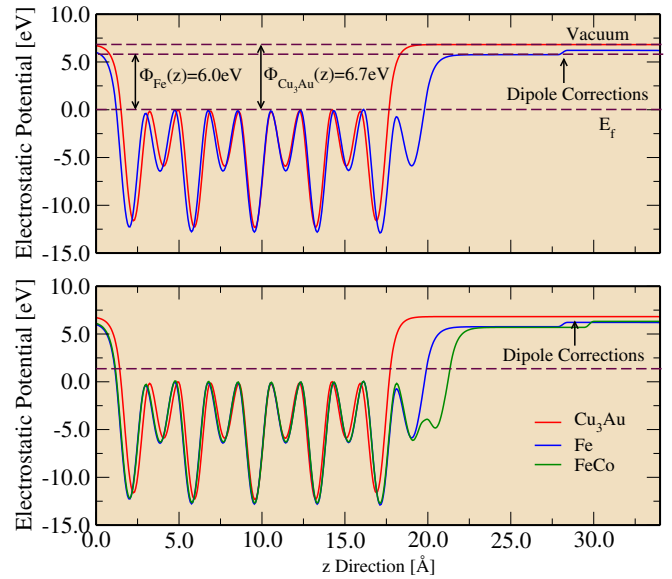

FIG. 9. Calculated electrostatic potential as a function of growth direction (z). The difference between the electrostatic potential and Fermi energy is the work function (Φ), calculated for Cu$_3$Au(001) and Fe(001) deposited MLs (top panel) and Cu$_3$Au(001) and FeCo(001) deposited MLs (bottom panel).

Fe (blue line) and FeCo (green line) magnetic layers. The work function [$\Phi(z)$] is defined as the difference between the vacuum (E_v) and Fermi (E_f) electrostatic potential energies, $\Phi_f(z) = E_v - E_f$. The work function is the energy required to remove one electron from the slab to the vacuum region. As expected, the higher work function of the unpolarized material [$\Phi(z) = 6.70$ eV] indicates that it is easier to remove one electron from the surface with one ML Fe deposited [$\Phi(z) = 6.00$ eV]. Thus, by performing the deposition of the magnetic ML on the NM surface, the work function decreases (Fig. 9, top panel). However, increasing the number of the magnetic MLs further, the work function remains practically the same (Fig. 9, bottom panel). This result goes in line with the deposited magnetic structures, which are stable but less stable than the Cu$_3$Au(001) surface. In addition, a small misalignment in the growth direction between the work function of the structures without magnetic overlayer and with one deposited iron ML was observed, while the surface with two magnetic MLs shows practically the same behavior of one deposited iron ML. This difference is more pronounced at the surface of the Cu$_3$Au(001) and disappears in the center of the slab, which tends to the bulklike behavior, depicting the corrugation reported in Fig. 2.

B. Spin-charge density investigations

DFT allows one to converge the charge density for the FeCo/Cu$_3$Au(001) polarized system. The spin-charge density (the difference between the spins majority and minority) displays the MMs which are localized on a specific atom. In our case, the spin-charge density investigation indicates the induction of the MM in the Cu and Au atoms due to the deposition of the magnetic layers. The results for one ML Fe (left) and Co (right) are presented in Fig. 10. As expected,
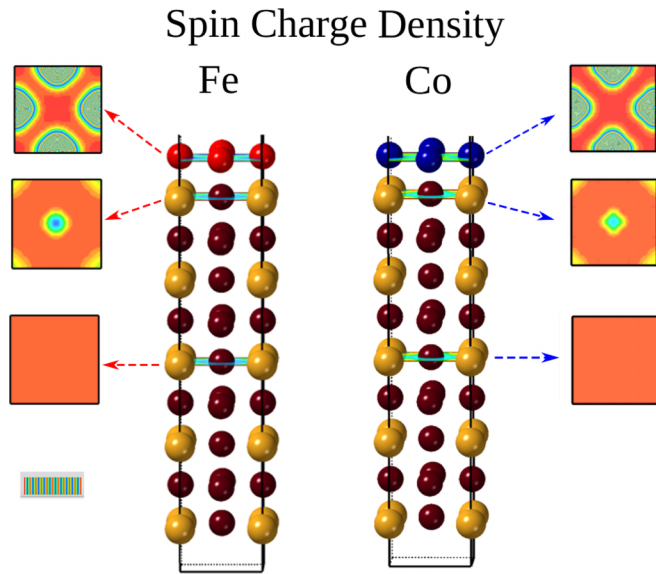
Spin Charge Density

FIG. 10. Charge-density calculations. The horizontal planes indicate the spin-charge density for Fe, in left panel, and Co, in the right panel.

FIG. 11. Effective Bader charges for the $Cu_3Au(001)$ surface atoms (Q_{eff}^{Cu-T}) and (Q_{eff}^{Au-T}), and also for copper (Q_{ef}^{Cu-C}) and gold (Q_{eff}^{Au-C}) atoms in the center of the slab, as a function of the number of deposited magnetic MLs. The left panel shows magnetic deposition when the first ML is composed by Fe (A1) and the right panel displays the case of first Co (B1) ML. The surface without Fe (Co) magnetic ML is indicated by A0 (B0) and the deposition starts with one ML A1 (B1) up to five MLs A5 (B5).

the spin-charge density calculations show the strong MM for Co and Fe atoms, as represented by the surface image at the magnetic ML planes. It is worth noticing that the MMs are almost circular, representing the orbitals and the chemical bonds where the electrons can be found. In addition, the decrease of induced MMs in the Cu and Au surface atoms and MMs induction were clearly noted, vanishing in the plane of the central atoms of the calculated slab, where this region shows the same trends of the bulk phase. The regions denoted by yellow and green colors in the horizontal planes of the spin-charge density indicate the magnetic induction in the gold and copper, where the Cu atoms suffer a higher MM induction than the Au atoms. The orange regions show the absence of MM. Also, the induced MMs in the $Cu_3Au(001)$ surface atoms are higher when the first deposited magnetic ML is composed by iron atoms. The distance between each plane of atoms and the atomic positions in the slab determine the hybridization between the top and bottom MLs, changing the values of the MMs.

C. Charge flow: Bader analysis

The induced MMs in the Cu and Au surface atoms modify the chemical environment surrounding these interface atoms. The hybridization between the NM and magnetic atoms of the interface changes the electron occupations and the electron density of the slab, altering the electron-electron and electron-ion Coulomb interactions, revealing a charge transfer between the interface atoms. In consequence, the atoms of the calculated slab show a new electronegativity and electropositivity when the magnetic atoms are deposited on the NM surface. This new chemical environment is investigated by the Bader charge [91] calculation, which is an investigation of electron density topology [92,93]. Thus, we investigated the charge flow in the $Cu_3Au(001)$ surface atoms due to the magnetic layer deposition. The effective Bader charge (Q_{eff}^B) is given
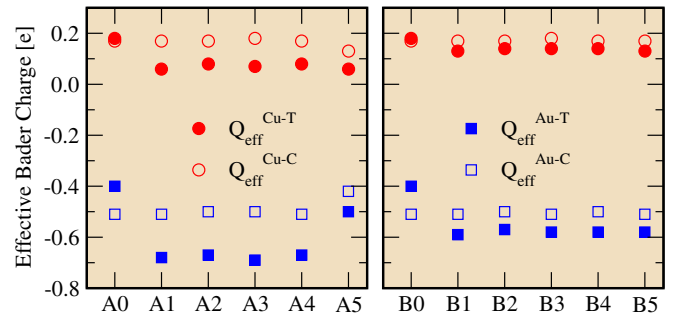
by the difference between the electrons valence (Z_{val}) and the charge confined in the Bader volume (Q^B), $Q_{eff}^B = Z_{val} - Q^B$. The left panel of Fig. 11 depicts the effective Bader charge for Stack A (Fe, the first ML) and the right panel displays the case of Stack B (Co, the first ML). The results are also reported in Table S3 of the Supplemental Material [90], where in the upper (bottom) part are the results for the iron (cobalt) in the first deposited ML. The charge transfer in the copper (Cu-T) and gold (Au-T) surface atoms is reached when the magnetic MLs are deposited on the $Cu_3Au(001)$ surface. The effective Bader charge for the pristine $Cu_3Au(001)$ surface atoms is $0.18\,e$ and $-0.40\,e$ for Cu-T and Au-T, respectively, indicating that the gold attracts more charge density around it than the copper atoms. Moreover, when the first iron ML is deposited, the Cu-T becomes less electropositive ($0.06\,e$), while the Au-T ($-0.68\,e$) becomes more electronegative in comparison with the $Cu_3Au(001)$ without the magnetic material deposition. Also, when the first magnetic ML is composed by cobalt atoms, the effective Bader charges for Cu-T and Au-T are $0.13\,e$ and $-0.59\,e$, respectively. Thus, in this case, the changes in effective Bader charge for Au-T are greater in comparison with the case when Fe is deposited on the NM surface. The first magnetic ML induces a charge transfer in the $Cu_3Au(001)$ surface atoms, with Cu-T (Au-T), becoming more cationic (anionic). Also, the modification of the effective Bader charge is mainly due to the first magnetic ML, and more ML depositions do not change the effective Bader charge significantly. The effective Bader charges in the center of the slab for copper (Cu-C) and gold (Au-C) are very similar to the effective Bader charges for the structure without the magnetic MLs. Thus, these findings further confirm that the charge transfer occurs only in the surface atoms, in accordance with our spin-charge density investigations (see Fig. 10).

IV. CONCLUSIONS

The understanding of local magnetic moment formation in materials is crucial to designing new nanodevice applications. The control of the MM in heterostructured materials is crucial

to functionalize the magnetic properties of interest. However, a comprehensive characterization of localized MMs in spin-polarized structures grown on magnetic and NM structures, and of proximity effects in FM/NM interfaces is still limited in the literature. Using theoretical investigations at atomistic level within density functional theory, a systematic study of the evolution of the MMs due to the epitaxial growth of alternate Fe and Co monoatomic layers, up to six MLs, starting with either metal, and as a function of the number of magnetic layers was performed aiming also to understand the induction of MMs on the $Cu_3Au(001)$ surface atoms. We found that the deposition of the Fe/Co magnetic stacks on the NM surface induces a localized MM in the Cu and Au atoms of the $Cu_3Au(001)$ surface. Also, the induced MM is stronger when the first magnetic MLs are composed by Fe atoms. In addition, by increasing the number of magnetic MLs, an oscillation of the average MMs as a function of thickness was observed. Finally, the charge calculations within the spin-charge density

and effective Bader charge confirm the induced MM in the Cu and Au of $Cu_3Au(001)$ surface atoms. Our results show good agreement with available experimental data [41,89] for Fe, Co, and Cu atoms in alternate Fe/Co on $Cu_3Au(001)$.

[1] M. Goto, Y. Wakatake, U. K. Oji, S. Miwa, N. Strelkov, B. Dieny, H. Kubota, K. Yakushiji, A. Fukushima, S. Yuasa, and Y. Suzuki, Microwave amplification in a magnetic tunnel junction induced by heat-to-spin conversion at the nanoscale, Nat. Nanotechnol. **14**, 40 (2019).

[2] E. Raymenants, O. Bultynck, D. Wan, T. Devolder, K. Garello, L. Souriau, A. Thiam, D. Tsvetanova, Y. Canvel, D. E. Nikonov, I. A. Young, M. Heyns, B. Soree, I. Asselberghs, I. Radu, S. Couet, and V. D. Nguyen, Nanoscale domain wall devices with magnetic tunnel junction read and write, Nat. Electron. **4**, 392 (2021).

[3] E. M. Palmero, M. Méndez, S. González, C. Bran, V. Vega, M. Vázquez, and V. M. Prida, Stepwise magnetization reversal of geometrically tuned in diameter Ni and FeCo bi-segmented nanowire arrays, Nano Res. **12**, 1547 (2019).

[4] T. Hasegawa, T. Niibori, Y. Takemasa, and M. Oikawa, Stabilisation of tetragonal FeCo structure with high magnetic anisotropy by the addition of V and N elements, Sci. Rep. **9**, 5248 (2019).

[5] M. Melzer, D. Makarov, and O. G. Schmidt, A review on stretchable magnetic field sensorics, J. Phys. D: Appl. Phys. **53**, 083002 (2020).

[6] P. M. Martins, A. C. Lima, S. Ribeiro, S. Lanceros-Mendez, and P. Martins, Magnetic nanoparticles for biomedical applications: From the soul of the Earth to the deep history of ourselves, ACS Appl. Bio Mater. **4**, 5839 (2021).

[7] S. Khizar, N. M. Ahmad, N. Zine, N. Jaffrezic-Renault, A. Errachid-el salhi, and A. Elaissari, Magnetic nanoparticles: From synthesis to theranostic applications, ACS Appl. Mater. Interfaces **4**, 4284 (2021).

[8] S.-h. Kong, T. Okamoto, and S. Nakagawa, Improvement of soft magnetic properties of Fe-Co-B underlayer with large saturation magnetization by Ni-Fe-O seedlayers, J. Appl. Phys. **93**, 6778 (2003).

[9] H. Wu, Y. Xu, P. Deng, Q. Pan, S. A. Razavi, K. Wong, L. Huang, B. Dai, Q. Shao, G. Yu, X. Han, J.-C. Rojas-Sánchez, S. Mangin, and K. L. Wang, Spin-orbit torque switching of a

nearly compensated ferrimagnet by topological surface states, Adv. Mater. **31**, 1901681 (2019).

[10] Z. Shang, T. Liu, Q. Yang, S. Cui, K. Xu, Y. Zhang, J. Deng, T. Zhai, and X. Wang, Chiral-molecule-based spintronic devices, Small **18**, 2203015 (2022).

[11] C. Holzmann, A. Ullrich, O.-T. Ciubotariu, and M. Albrecht, Stress-induced magnetic properties of gadolinium iron garnet nanoscale-thin films: Implications for spintronic devices, ACS Appl. Nano Mater. **5**, 1023 (2022).

[12] C. Song, X. Li, L. Shen, B. Cui, X. Xu, G. Yu, M. Liu, S. Meng, and K. Wu, Emergent perpendicular magnetic anisotropy at the interface of an oxide heterostructure, Phys. Rev. B **104**, 115162 (2021).

[13] J. F. Sierra, J. Fabian, R. K. Kawakami, S. Roche, and S. O. Valenzuela, Van der Waals heterostructures for spintronics and opto-spintronics, Nat. Nanotechnol. **16**, 856 (2021).

[14] G. Wu, D. Wang, N. Verma, R. Rao, Y. Cheng, S. Guo, G. Cao, K. Watanabe, T. Taniguchi, C. N. Lau, F. Yang, M. Randeria, M. Bockrath, and P. C. Hammel, Enhancing perpendicular magnetic anisotropy in garnet ferrimagnet by interfacing with few-layer WTe_2, Nano Lett. **22**, 1115 (2022).

[15] Y. Kim, W. Jeong, D. Yun, G.-E. Ahn, and O. Lee, Spin and orbital properties of perpendicular magnetic anisotropy for spin-orbit torque material devices, Appl. Surf. Sci. **544**, 148959 (2021).

[16] M. Blanco-Rey, P. Perna, A. Gudin, J. M. Diez, A. Anadón, P. Olleros-Rodríguez, L. de Melo Costa, M. Valvidares, P. Gargiani, A. Guedeja-Marron, M. Cabero, M. Varela, C. García-Fernández, M. M. Otrokov, J. Camarero, R. Miranda, A. Arnau, and J. I. Cerdá, Large perpendicular magnetic anisotropy in nanometer-thick epitaxial graphene/Co/heavy metal heterostructures for spin–orbitronics devices, ACS Appl. Nano Mater. **4**, 4398 (2021).

[17] T. Burkert, L. Nordström, O. Eriksson, and O. Heinonen, Giant Magnetic Anisotropy in Tetragonal FeCo Alloys, Phys. Rev. Lett. **93**, 027203 (2004).

[18] D. Odkhuu and S. C. Hong, First-Principles Prediction of Possible Rare-Earth Free Permanent Magnet of Tetragona FeCo with

Enhanced Magnetic Anisotropy and Energy Product through Interstitial Nitrogen, Phys. Rev. Appl. **11**, 054085 (2019).

[19] A. L. Wysocki, M. C. Nguyen, C.-Z. Wang, K.-M. Ho, A. V. Postnikov, and V. P. Antropov, Concentration-tuned tetragonal strain in alloys: Application to magnetic anisotropy of $FeNi_{1-x}Co_x$, Phys. Rev. B **100**, 104429 (2019).

[20] L. Cabral, F. H. Aragón, L. Villegas-Lelovsky, M. P. Lima, W. A. A. Macedo, and J. L. F. Da Silva, Tuning the magnetic properties of FeCo thin films through the magnetoelastic effect induced by the Au underlayer thickness, ACS Appl. Mater. Interfaces **11**, 1529 (2019).

[21] Y. Kota and A. Sakuma, Degree of order dependence on magnetocrystalline anisotropy in body-centered tetragonal FeCo alloys, Appl. Phys. Express **5**, 113002 (2012).

[22] S. Okamoto, N. Kikuchi, O. Kitakami, T. Miyazaki, Y. Shimada, and K. Fukamichi, Chemical-order-dependent magnetic anisotropy and exchange stiffness constant of FePt(001) epitaxial films, Phys. Rev. B **66**, 024413 (2002).

[23] M. Si, A. Izardar, and C. Ederer, Effect of chemical disorder on the magnetic anisotropy in $L1_0$ FeNi from first-principles calculations, Phys. Rev. Res. **4**, 033161 (2022).

[24] C. Brombacher, H. Schletter, M. Daniel, P. Matthes, N. Jöhrmann, M. Maret, D. Makarov, M. Hietschold, and M. Albrecht, FePtCu alloy thin films: Morphology, $L1_0$ chemical ordering, and perpendicular magnetic anisotropy, J. Appl. Phys. **112**, 073912 (2012).

[25] K. Abe, S. Wu, Y. Tanaka, Y. Ariake, I. Kanada, T. Mewes, G. Mankey, C. Mewes, and T. Suzuki, The thickness and growth temperature dependences of soft magnetic properties and an effective damping parameter of (FeCo)-Si alloy thin films, AIP Adv. **9**, 035139 (2019).

[26] S. Nayak, B. B. Singh, S. Mallick, and S. Bedanta, Tuning of magnetic properties by alternating the order of hard/soft bilayers with various thicknesses, J. Phys. D: Appl. Phys. **52**, 305301 (2019).

[27] S. Wu, K. Abe, T. Nakano, T. Mewes, C. Mewes, G. J. Mankey, and T. Suzuki, Thickness dependence of dynamic magnetic properties of soft (FeCo)-Si alloy thin films, Phys. Rev. B **99**, 144416 (2019).

[28] A. S. Kebaili, S. Blizak, G. Bihlmayer, and S. Blügel, Magnetic properties of ultra-thin (Fe, Co) films coupled by Ir(001) spacers, Phys. B: Condens. Matter **596**, 412395 (2020).

[29] W. A. A. Macedo, W. Keune, and E. D. Ellerbrock, Magnetic properties of ultrathin epitaxial fcc-Fe(001) films on Cu(001) and $Cu_3Au(001)$, J. Magn. Magn. Mater. **93**, 552 (1991).

[30] J. Okabayashi, T. Koyama, M. Suzuki, M. Tsujikawa, M. Shirai, and D. Chiba, Induced perpendicular magnetization in a Cu layer inserted between Co and Pt layers revealed by x-ray magnetic circular dichroism, Sci. Rep. **7**, 46132 (2017).

[31] S. Nicolodi, L. Nagamine, A. Viegas, J. Schmidt, L. Pereira, C. Deranlot, F. Petroff, and J. Geshev, Copper spacer thickness dependence of the exchange bias in IrMn/Cu/Co ultrathin films, J. Magn. Magn. Mater. **316**, e97 (2007).

[32] B. Kocaman, K. Yildiz Aktaş, and A. C. Basaran, Dependence of exchange bias and coercive field on Cu spacer thickness in oblique deposited Co/Cu/CoO multilayers, J. Magn. Magn. Mater. **530**, 167926 (2021).

[33] X. Li and C. S. Lynch, Strong electric field tuning of magnetism in self-biased multiferroic structures, Sci. Rep. **10**, 21148 (2020).

[34] Z.-W. Lai, Theory of ordering dynamics for Cu_3Au, Phys. Rev. B **41**, 9239 (1990).

[35] G. K. Wertheim, L. F. Mattheiss, and D. N. E. Buchanan, Partial densities of states of ordered Cu_3Au, Phys. Rev. B **38**, 5988 (1988).

[36] L.-X. Ye, R. C. Bhatt, C.-M. Lee, W.-H. Hsu, and T. ho Wu, Perpendicular magnetic anisotropy in TbFeCo/MgO structure with Ta- and Hf-underlayer, J. Magn. Magn. Mater. **502**, 166554 (2020).

[37] K. Liu, S. Zhang, D. Wu, L. Luo, X. Sun, X. Chen, D. Zakharov, S. Cheng, Y. Zhu, J. C. Yang, G. Wang, and G. Zhou, Effect of surface steps on chemical ordering in the subsurface of Cu(Au) solid solutions, Phys. Rev. B **103**, 035401 (2021).

[38] W. A. A. Macedo, P. L. Gastelois, M. D. Martins, W. Kuch, J. Miguel, and M. Y. Khan, Growth, structure, and magnetic properties of epitaxial Ni_xMn_{100-x} single layers and Co/Ni_xMn_{100-x} bilayers on Cu_3Au, Phys. Rev. B **82**, 134423 (2010).

[39] M. Wolloch and D. Suess, Strain-induced control of magnetocrystalline anisotropy energy in FeCo thin films, J. Magn. Magn. Mater. **522**, 167542 (2021).

[40] T. Ohtsuki, T. Kojima, M. Kotsugi, T. Ohkochi, M. Mizuguchi, and K. Takanashi, Magnetic domain observation of FeCo thin films fabricated by alternate monoatomic layer deposition, J. Appl. Phys. **115**, 043908 (2014).

[41] A. S. Ponce, S. O. Parreiras, A. A. C. Cotta, G. F. M. Gomes, P. Schio, J. C. Cezar, R. Paniago, P. L. Gastelois, and W. A. A. Macedo, Chemical order and magnetic anisotropy in alternate Fe/Co monolayers on $Cu_3Au(001)$, AIP Adv. **8**, 115307 (2018).

[42] L. Reichel, A. Edström, D. Pohl, J. Rusz, O. Eriksson, L. Schultz, and S. Fäler, On the origin of perpendicular magnetic anisotropy in strained Fe-Co-X films, J. Phys. D: Appl. Phys. **50**, 045003 (2017).

[43] H. Ito, M. Saito, T. Miyamachi, F. Komori, T. Koganezawa, M. Mizuguchi, and M. Kotsugi, Fabrication of $L1_0$-type FeCo ordered structure using a periodic Ni buffer layer, AIP Adv. **9**, 045307 (2019).

[44] N. Lei, L. Yang, D. Wei, Y. Tian, and X. Jin, Extraction of the chemical contribution to the interfacial magnetic anisotropy in $Ni/Cu_3Au(001)$, Phys. Rev. B **105**, 024402 (2022).

[45] J. E. Hirsch, Spin Hall Effect, Phys. Rev. Lett. **83**, 1834 (1999).

[46] M. Dyakonov and V. Perel, Current-induced spin orientation of electrons in semiconductors, Phys. Lett. A **35**, 459 (1971).

[47] E. C. Ahn, 2D materials for spintronic devices, npj 2D Mater. Appl. **4**, 17 (2020).

[48] A. Hirohata and K. Takanashi, Future perspectives for spintronic devices, J. Phys. D: Appl. Phys. **47**, 193001 (2014).

[49] Q. Shao, P. Li, L. Liu, H. Yang, S. Fukami, A. Razavi, H. Wu, K. Wang, F. Freimuth, Y. Mokrousov, M. D. Stiles, S. Emori, A. Hoffmann, J. Åkerman, K. Roy, J.-P. Wang, S.-H. Yang, K. Garello, and W. Zhang, Roadmap of spin-orbit torques, IEEE Trans. Magn. **57**, 1 (2021).

[50] X. F. Zhou, X. Z. Chen, J. Zhang, F. Li, G. Y. Shi, Y. M. Sun, M. S. Saleem, Y. F. You, F. Pan, and C. Song, From Fieldlike Torque to Antidamping Torque in Antiferromagnetic Mn_2Au, Phys. Rev. Appl. **11**, 054030 (2019).

[51] V. M. T. S. Barthem, C. V. Colin, H. Mayaffre, M.-H. Julien, and D. Givord, Revealing the properties of Mn_2Au for antiferromagnetic spintronics, Nat. Commun. **4**, 2892 (2013).

[52] A. A. Sapozhnik, M. Jourdan, H. Zabel, M. Kläui, and H.-J. Elmers, Exchange bias in epitaxial Mn$_2$Au(001)/Fe(001) bilayers, J. Phys. D: Appl. Phys. **52**, 465003 (2019).

[53] M. Jourdan, H. Bräuning, A. Sapozhnik, H.-J. Elmers, H. Zabel, and M. Kläui, Epitaxial Mn$_2$Au thin films for antiferromagnetic spintronics, J. Phys. D: Appl. Phys. **48**, 385001 (2015).

[54] J. Han, A. Richardella, S. A. Siddiqui, J. Finley, N. Samarth, and L. Liu, Room-Temperature Spin-Orbit Torque Switching Induced by a Topological Insulator, Phys. Rev. Lett. **119**, 077702 (2017).

[55] G. Wu, D. Wu, Y. Ren, Q. Y. Jin, and Z. Zhang, Topological surface state manipulation of magnetic damping and surface anisotropy in topological insulator/nonmagnet/CoFe heterostructures, Phys. Rev. B **103**, 014419 (2021).

[56] Q. Chen, L. Cao, J. Li, Q. Fu, Y. Zhu, Q. Guo, R. Liu, T. Li, W. Zhang, J. Du, J. Zheng, Z. Huang, P. K. J. Wong, B. Fang, Z. Zeng, and Y. Zhai, Effective tuning of spin mixing conductance at the Py/Cu-Nd interface, Appl. Phys. Lett. **120**, 242405 (2022).

[57] C.-Y. Hu, Y.-F. Chiu, C.-C. Tsai, C.-C. Huang, K.-H. Chen, C.-W. Peng, C.-M. Lee, M.-Y. Song, Y.-L. Huang, S.-J. Lin, and C.-F. Pai, Toward 100% spin-orbit torque efficiency with high spin-orbital Hall conductivity Pt-Cr alloys, ACS Appl. Electron. Mater. **4**, 1099 (2022).

[58] S. Selzer, L. Salemi, A. Deák, E. Simon, L. Szunyogh, P. M. Oppeneer, and U. Nowak, Current-induced switching of antiferromagnetic order in Mn$_2$Au from first principles, Phys. Rev. B **105**, 174416 (2022).

[59] V. Grigorev, M. Filianina, S. Y. Bodnar, S. Sobolev, N. Bhattacharjee, S. Bommanaboyena, Y. Lytvynenko, Y. Skourski, D. Fuchs, M. Kläui, M. Jourdan, and J. Demsar, Optical Readout of the Néel Vector in the Metallic Antiferromagnet Mn$_2$Au, Phys. Rev. Appl. **16**, 014037 (2021).

[60] H.-C. Wu, Z.-M. Liao, R. G. S. Sofin, G. Feng, X.-M. Ma, A. B. Shick, O. N. Mryasov, and I. V. Shvets, Mn$_2$Au: Body-centered-tetragonal bimetallic antiferromagnets grown by molecular beam epitaxy, Adv. Mater. **24**, 6374 (2012).

[61] T. Okuno, D.-H. Kim, S.-H. Oh, S. K. Kim, Y. Hirata, T. Nishimura, W. S. Ham, Y. Futakawa, H. Yoshikawa, A. Tsukamoto, Y. Tserkovnyak, Y. Shiota, T. Moriyama, K.-J. Kim, K.-J. Lee, and T. Ono, Spin-transfer torques for domain wall motion in antiferromagnetically coupled ferrimagnets, Nat. Electron. **2**, 389 (2019).

[62] L. Zhu, L. Zhu, X. Ma, X. Li, and R. A. Buhrman, Critical role of orbital hybridization in the Dzyaloshinskii-Moriya interaction of magnetic interfaces, Commun. Phys. **5**, 151 (2022).

[63] F. Hellman, A. Hoffmann, Y. Tserkovnyak, G. S. D. Beach, E. E. Fullerton, C. Leighton, A. H. MacDonald, D. C. Ralph, D. A. Arena, H. A. Dürr, P. Fischer, J. Grollier, J. P. Heremans, T. Jungwirth, A. V. Kimel, B. Koopmans, I. N. Krivorotov, S. J. May, A. K. Petford-Long, J. M. Rondinelli *et al.*, Interface-induced phenomena in magnetism, Rev. Mod. Phys. **89**, 025006 (2017).

[64] H. S. Jung, W. D. Doyle, J. E. Wittig, J. F. Al-Sharab, and J. Bentley, Soft anisotropic high magnetization Cu/FeCo films, Appl. Phys. Lett. **81**, 2415 (2002).

[65] F. Yu, Y. Zheng, M. Mitsunori, L. Xiao-Xi, and M. Akimitsu, Studies on high-moment soft magnetic FeCo/Co thin films, Chin. Phys. **15**, 1351 (2006).

[66] B. Újfalussy, L. Szunyogh, P. Bruno, and P. Weinberger, First-Principles Calculation of the Anomalous Perpendicular Anisotropy in a Co Monolayer on Au(111), Phys. Rev. Lett. **77**, 1805 (1996).

[67] S. Caspani, S. Moraes, D. Navas, M. P. Proenca, R. Magalhães, C. Nunes, J. a. P. Araújo, and C. T. Sousa, The magnetic properties of Fe/Cu multilayered nanowires: The role of the number of Fe layers and their thickness, Nanomaterials **11**, 2729 (2021).

[68] M. G. Samant, J. Stöhr, S. S. P. Parkin, G. A. Held, B. D. Hermsmeier, F. Herman, M. van Schilfgaarde, L.-C. Duda, D. C. Mancini, N. Wassdahl, and R. Nakajima, Induced Spin Polarization in Cu Spacer Layers in Co/Cu Multilayers, Phys. Rev. Lett. **72**, 1112 (1994).

[69] V. Vas'kovskiy, A. Svalov, A. Gorbunov, N. Schegoleva, and S. Zadvorkin, Structure and magnetic properties of Gd/Si and Gd/Cu multilayered films, Phys. B: Condens. Matter **315**, 143 (2002).

[70] S. Bandiera, R. C. Sousa, B. Rodmacq, L. Lechevallier, and B. Dieny, Effect of a Cu spacer between Co and Pt layers on the structural and magnetic properties in (Co/Cu/Pt)$_5$/Pt type multilayers, J. Phys. D: Appl. Phys. **46**, 485003 (2013).

[71] P. Swaminathan, R. A. Rosenberg, G. K. Shenoy, J. S. Palmer, and J. H. Weaver, Induced magnetism in Cu nanoparticles embedded in Co, Appl. Phys. Lett. **91**, 202506 (2007).

[72] J. Okabayashi, S. Li, S. Sakai, Y. Kobayashi, T. Mitsui, K. Tanaka, Y. Miura, and S. Mitani, Perpendicular magnetic anisotropy at the Fe/Au(111) interface studied by Mössbauer, x-ray absorption, and photoemission spectroscopies, Phys. Rev. B **103**, 104435 (2021).

[73] J. Okabayashi, S. Li, S. Sakai, Y. Kobayashi, K. Fujiwara, T. Mitsui, and S. Mitani, Mössbauer spectroscopy with polarized synchrotron beams at Fe/Au(111) interface, Hyperfine Interact. **242**, 59 (2021).

[74] S. O. Parreiras, L. A. Cabral, R. V. Lourenço, A. A. Cotta, P. Schio, J. C. Cezar, P. L. Gastelois, E. Z. da Silva, and W. A. A. Macedo, Induced magnetization in Cu atoms at the Fe-Co/Cu$_3$Au(001) interface: X-ray magnetic circular dichroism experiments and theoretical results, Appl. Surf. Sci. **548**, 149215 (2021).

[75] B. Sampedro, P. Crespo, A. Hernando, R. Litrán, J. C. Sánchez López, C. López Cartes, A. Fernandez, J. Ramírez, J. González Calbet, and M. Vallet, Ferromagnetism in fcc Twinned 2.4 nm Size Pd Nanoparticles, Phys. Rev. Lett. **91**, 237203 (2003).

[76] W. Kohn and L. J. Sham, Self-consistent equations including exchange and correlation effects, Phys. Rev. **140**, A1133 (1965).

[77] J. P. Perdew, J. A. Chevary, S. H. Vosko, K. A. Jackson, M. R. Pederson, D. J. Singh, and C. Fiolhais, Atoms, molecules, solids, and surfaces: Applications of the generalized gradient approximation for exchange and correlation, Phys. Rev. B **46**, 6671 (1992).

[78] J. P. Perdew, K. Burke, and M. Ernzerhof, Generalized Gradient Approximation Made Simple, Phys. Rev. Lett. **77**, 3865 (1996).

[79] J. P. Perdew, K. Burke, and M. Ernzerhof, Generalized Gradient Approximation Made Simple, Phys. Rev. Lett. **77**, 3865 (1996), Phys. Rev. Lett. **78**, 1396(E) (1997).

[80] I. Turek, J. Kudrnovský, and K. Carva, Magnetic anisotropy energy of disordered tetragonal Fe–Co systems from *ab initio* alloy theory, Phys. Rev. B **86**, 174430 (2012).

[81] Y. Wei, Y.-Y. Sun, J. Yang, S.-J. Gong, Y.-H. Meng, and C.-G. Duan, First-principles investigation of the interface magnetic anisotropy of Fe/SrTiO$_3$, J. Phys.: Condens. Matter **31**, 075803 (2019).

[82] P. E. Blöchl, Projector augmented-wave method, Phys. Rev. B **50**, 17953 (1994).

[83] G. Kresse and D. Joubert, From ultrasoft pseudopotentials to the projector augmented-wave method, Phys. Rev. B **59**, 1758 (1999).

[84] G. Kresse and J. Hafner, *Ab Initio* molecular dynamics for open-shell transition metals, Phys. Rev. B **48**, 13115 (1993).

[85] G. Kresse and J. Furthmüller, Efficient iterative schemes for *Ab Initio* total-energy calculations using a plane-wave basis set, Phys. Rev. B **54**, 11169 (1996).

[86] D. Hobbs, G. Kresse, and J. Hafner, Fully unconstrained noncollinear magnetism within the projector augmented-wave method, Phys. Rev. B **62**, 11556 (2000).

[87] S. Steiner, S. Khmelevskyi, M. Marsmann, and G. Kresse, Calculation of the magnetic anisotropy with projected-augmented-wave methodology and the case study of disordered Fe$_{1-x}$Co$_x$ alloys, Phys. Rev. B **93**, 224425 (2016).

[88] O. K. Andersen, Linear methods in band theory, Phys. Rev. B **12**, 3060 (1975).

[89] A. A. C. Cotta, D. V. P. Massote, G. A. S. Ribeiro, G. C. S. Valadares, R. B. Capaz, E. A. Soares, and W. A. A. Macedo, A combined LEED and DFT surface structure determination of Cu$_3$Au(001): Evidence of a surface stacking fault, Surf. Sci. **618**, 167 (2013).

[90] See Supplemental Material at http://link.aps.org/supplemental/10.1103/PhysRevB.106.214430 for evolution of the Fe-Co magnetism and magnetic proximity effects in alternate Fe/Co monolayers on non-magnetic Cu$_3$Au(001).

[91] R. Bader, *Atoms in Molecules: A Quantum Theory*, International Series of Monographs on Chemistry (Clarendon, Oxford, 1994).

[92] G. Henkelman, A. Arnaldsson, and H. Jónsson, A fast and robust algorithm for Bader decomposition of charge density, Comput. Mater. Sci. **36**, 354 (2006).

[93] W. Tang, E. Sanville, and G. Henkelman, A grid-based Bader analysis algorithm without lattice bias, J. Phys.: Condens. Matter **21**, 084204 (2009).